

# Euryale Ferox Seed-Inspired Superlubricated Nanoparticles for Treatment of Osteoarthritis

Yufei Yan, Tao Sun, Hongbo Zhang, Xiuling Ji, Yulong Sun, Xin Zhao, Lianfu Deng, Jin Qi, Wenguo Cui, Hélder A. Santos, Hongyu Zhang

## Abstract

Osteoarthritis has been regarded as a typical lubrication deficiency related joint disease, which is characterized by the breakdown of articular cartilage at the joint surface and the inflammation of the joint capsule. Here, inspired by the structure of the fresh euryale ferox seed that possesses a slippery aril and a hard coat containing starchy kernel, a novel superlubricated nanoparticle, namely poly (3-sulfopropyl methacrylate potassium salt)-grafted mesoporous silica nanoparticles (MSNs-NH<sub>2</sub>@PSPMK), is biomimicked and synthesized via a one-step photopolymerization method. The nanoparticles are endowed with enhanced lubrication by the grafted PSPMK polyelectrolyte polymer due to the formation of tenacious hydration layers surrounding the negative charges, and simultaneously are featured with effective drug loading and release behavior as a result of the sufficient mesoporous channels in the MSNs. When encapsulated with an anti-inflammatory drug diclofenac sodium (DS), the lubrication capability of the superlubricated nanoparticles is improved, while the drug release rate is sustained by increasing the thickness of PSPMK layer, which is simply achieved via adjustment of the precursor monomer concentration in the photopolymerization process. Additionally, the *in vitro* and *in vivo* experimental results show that the DS-loaded MSNs-NH<sub>2</sub>@PSPMK nanoparticles effectively protect the chondrocytes from degeneration, and thus, inhibit the development of osteoarthritis.

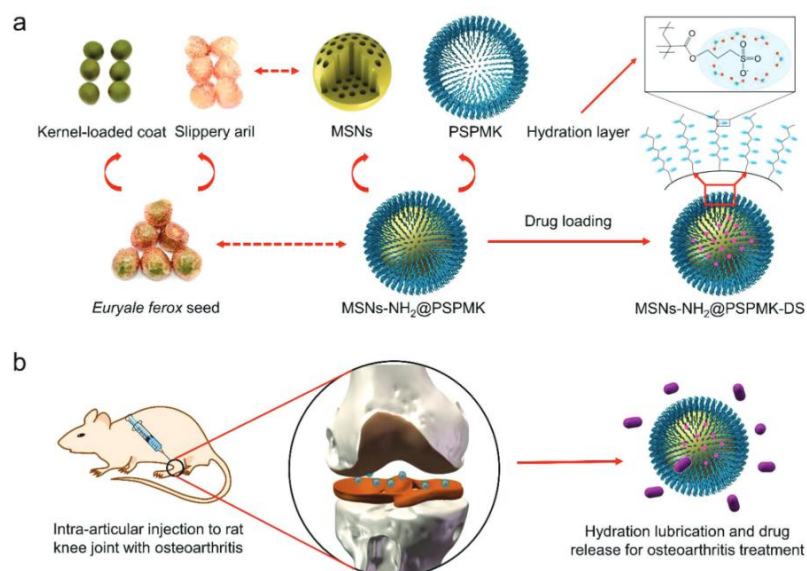
## 1 Introduction

From an engineering point of view, osteoarthritis has been regarded as a lubrication deficiency related joint disease triggered by breakdown of articular cartilage and inflammation of the joint, and it is considered that a synergetic therapy combining both lubrication and drug intervention predicts a promising nonsurgical strategy for treatment of osteoarthritis.<sup>1, 2</sup> Euryale ferox, also known as foxnut or makhana, is a flowering plant classified in the family of Nymphaeaceae. The fresh euryale ferox seed is composed of a membranous aril outside and a hard coat inside containing starchy kernel.<sup>3, 4</sup> The streaked bright red membranous aril is very slippery and slimy in nature, while the hard coat loads the starchy kernel which can be used for the treatment of articular joint pain. Accordingly, on the basis of inspiration from the structure of fresh euryale ferox seed, biomimetic nanoparticles may provide superlubricity on the outer surface and simultaneously drug loading in the inner core. Moreover, an intra-articular injection of such superlubricated drug-loaded nanoparticles into the joint can achieve both lubrication improvement during joint movement and drug intervene via local administration, and thus, be served as an effective treatment for osteoarthritis.

Mesoporous silica nanoparticles (MSNs) have long been recognized to be representative drug nanocarriers, owing to their large surface area, large pore volume, high thermal stability and good biocompatibility.<sup>5-9</sup> Incorporating superlubricated polymers onto the MSNs surface has been attempted as one of the most efficient and convenient approaches to construct multi-functional drug delivery systems with the feature of lubrication capability.<sup>10</sup> Various surface-grafted MSNs have been successfully developed for example, by different polymers via atom transfer radical polymerization,<sup>11, 12</sup> reversible addition-fragmentation chain transfer polymerization,<sup>13, 14</sup> and ring opening polymerization.<sup>15</sup> However, these methods can introduce toxic catalysts during the reaction, for example, the toxic metallic components in the process of atom transfer radical polymerization.<sup>16</sup> The toxic substances are difficult to be completely eliminated through postprocessing, consequently limiting the biological applications of such polymer-grafted MSNs. Additionally, so far few studies have investigated the lubrication capability of polymer-grafted MSNs and their biological applications where enhanced lubrication and sustained drug delivery are preferably desirable, e.g., treatment of osteoarthritis. Therefore, developing superlubricated drug-loaded MSNs without the involvement of complex synthesis and even the introduction of toxic catalysts is highly required but still remains a great challenge as yet.

Recently, hydration lubrication mechanism proposed by Klein has been accepted to dominate the scenario of the excellent superlubricity for articular cartilage.<sup>17, 18</sup> Particularly, it is considered that the hydration layers surrounding both the positive ( $N^+(CH_3)_3$ ) and negative ( $PO_4^-$ ) charges of the zwitterionic headgroups in the phosphatidylcholine lipids can bear typical joint pressures (4–10 MPa) with the friction coefficient at the joint interface at a level as low as 0.001–0.01. This is because the water molecules within the hydration layers are tenaciously held due to the interaction of the large water dipole with the enclosed charge, and will respond in a fluid-like manner when being sheared.<sup>19, 20</sup> Furthermore, various polyelectrolyte polymer brushes used to mimic the biomolecules of articular cartilage have been proved to significantly reduce friction coefficient based on the hydration lubrication mechanism.<sup>21-23</sup> Accordingly, in view of the excellent superlubricity behavior of the articular cartilage, grafting polyelectrolyte polymer brushes onto the MSNs surface may represent an effective approach to endow MSNs with enhanced lubrication capability.

In the present study, inspired by the unique structure of fresh *Euryale ferox* seed which consists of a slippery aril outside and a starchy kernel-loaded hard coat inside, we develop a facile and low-toxic photopolymerization method to synthesize superlubricated drug-loaded MSNs. As demonstrated in Scheme 1a, the slippery aril corresponds to the superlubricated polyelectrolyte polymer brushes, poly (3-sulfopropyl methacrylate potassium salt) (PSPMK), and the starchy kernel-loaded hard coat corresponds to the diclofenac sodium (DS)-loaded nanocarriers (MSNs-NH<sub>2</sub>@DS). We hypothesize that the superlubricated drug-loaded MSNs developed here, MSNs-NH<sub>2</sub>@PSPMK-DS, can be used as an effective intra-articular injective agent to inhibit the development of osteoarthritis, as shown in Scheme 1b.



**Scheme 1.** Schematic illustration showing a) the design of the superlubricated drug-loaded nanoparticles, MSNs-NH<sub>2</sub>@PSPMK-DS, which is bioinspired by the structure of fresh *euryale ferox* seed, and b) the in vitro and in vivo experiments, showing the treatment of osteoarthritis by MSNs-NH<sub>2</sub>@PSPMK-DS based on synergistic effect of enhanced lubrication and sustained drug release.

## 2 Results and Discussion

We biomimicked and synthesized superlubricated drug-loaded MSNs, MSNs-NH<sub>2</sub>@PSPMK-DS, for the treatment of osteoarthritis. For this we first prepared superlubricated nanoparticles, PSPMK-grafted MSNs (MSNs-NH<sub>2</sub>@PSPMK), by grafting SPMK monomer onto the surface of MSNs via photopolymerization, employing 2959-Tos as the initiator. Briefly, 2959-Tos was immobilized onto the surface of MSNs, and the resulting product (MSNs-NH<sub>2</sub>@I2959) was uniformly dispersed in SPMK monomer solution and reacted under UV-irradiation to obtain MSNs-NH<sub>2</sub>@PSPMK. Subsequently, MSNs-NH<sub>2</sub>@PSPMK were encapsulated with DS, a widely used nonsteroidal anti-inflammatory drug in clinics, to prepare MSNs-NH<sub>2</sub>@PSPMK-DS as a novel superlubricated drug-loaded nanoparticle. Similar to fresh *euryale ferox* seed, the polymer layer of MSNs-NH<sub>2</sub>@PSPMK-DS corresponding to the slippery aril was expected to endow the nanoparticles with lubrication capability, while DS-loaded MSNs corresponding to the starchy kernel-loaded hard coat to endow the nanoparticles with sustained drug release. The lubrication capability and drug release behavior of the nanoparticles can be easily tuned through controlling the thickness of the PSPMK layer by adjusting the monomer concentration in the photopolymerization process.

### 2.1 Characterization of Superlubricated Nanoparticles

Fourier transform infrared (FTIR) spectroscopy analysis was conducted to investigate the successful surface grafting reaction. As shown in Figure 1a, the spectra of MSNs, MSNs-NH<sub>2</sub>@I2959, and MSNs-NH<sub>2</sub>@PSPMK (0.500 m SPMK) all demonstrate the absorption band of Si-O-Si at 1093 cm<sup>-1</sup> and the stretching vibration of Si-OH at 3439 cm<sup>-1</sup>. Compared with MSNs, only slight differences are observed in the spectrum of MSNs-NH<sub>2</sub>@I2959, as the amount of photopolymerization initiator 2959-Tos modified on the MSNs surface is small. After the PSPMK polymer is grafted on the surface of MSNs, the absorption bands of S-O in SO<sub>3</sub>-

appear at 1045 and 1190  $\text{cm}^{-1}$ , and the absorption band of C=O appears at 1720  $\text{cm}^{-1}$ , as demonstrated from the spectrum of MSNs-NH<sub>2</sub>@PSPMK. The presence of these absorption bands confirms that PSPMK polyelectrolyte polymer has been successfully grafted on the MSNs surface via photopolymerization.

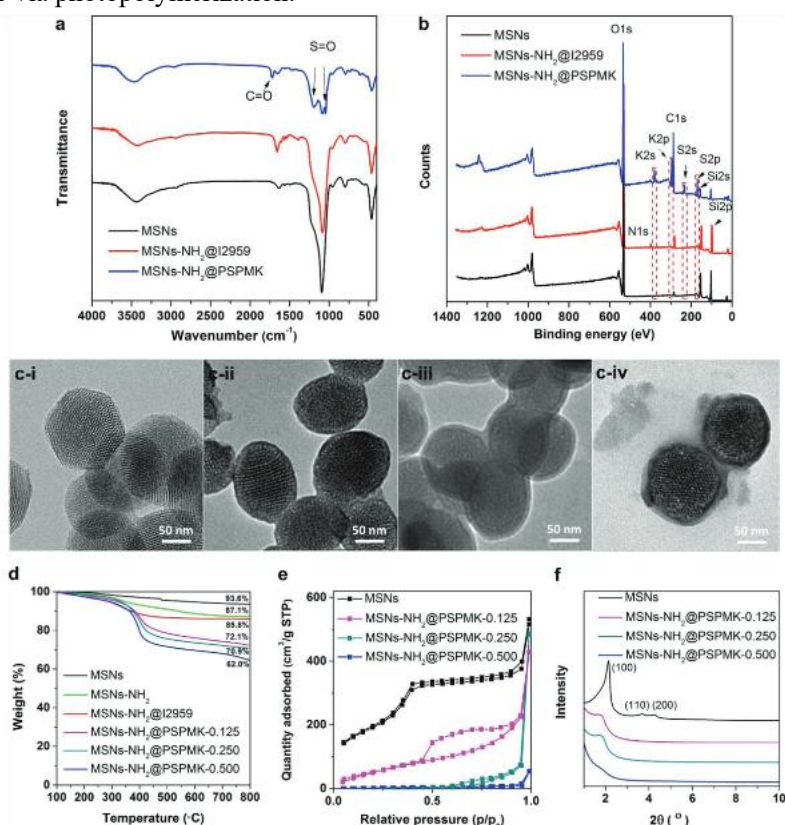


**Figure 1.** a) FTIR spectra and b) XPS spectra of MSNs, MSNs-NH<sub>2</sub>@I2959, and MSNs-NH<sub>2</sub>@PSPMK. c) The TEM images of MSNs and MSNs-NH<sub>2</sub>@PSPMK with three different SPMK monomer concentrations: c-i) MSNs; c-ii) MSNs-NH<sub>2</sub>@PSPMK-0.125; c-iii) MSNs-NH<sub>2</sub>@PSPMK-0.250; c-iv) MSNs-NH<sub>2</sub>@PSPMK-0.500. The thickness of the polymer layer is ~4, 7, and 9 nm, respectively. d) TGA curves, e) N<sub>2</sub> adsorption-desorption isotherm curves, and f) Small-angle XRD patterns of MSNs and MSNs-NH<sub>2</sub>@PSPMK with three different SPMK monomer concentrations.

Surface compositions of MSNs, MSNs-NH<sub>2</sub>@I2959, and MSNs-NH<sub>2</sub>@PSPMK (0.500 m SPMK) were also evaluated by X-ray photoelectron spectroscopy (XPS). As shown in Figure 1b, for MSNs, the binding energies of Si 2p and Si 2s are at 104 and 155 eV, respectively. For MSNs-NH<sub>2</sub>@I2959, the signal of N 1s at 398 eV is attributed to the introduction of amine groups on the MSNs surface. For MSNs-NH<sub>2</sub>@PSPMK, the grafting of the PSPMK polymer on the MSNs surface is confirmed by the signals of K and S elements appearing at 377 eV (K 2s), 293 eV (K 2p), 232 eV (S 2s), and 168 eV (S 2p).

Surface morphologies of MSNs and MSNs-NH<sub>2</sub>@PSPMK were observed using transmission electron microscopy (TEM). Figure 1c-i shows that MSNs have well-organized lattices, with an average diameter of about 114 nm. Figure 1c-ii-iv demonstrates MSNs-NH<sub>2</sub>@PSPMK prepared by photopolymerization with different SPMK monomer concentrations. It is evident that all the MSNs-NH<sub>2</sub>@PSPMK nanoparticles are surrounded by a shaded polymer layer, and the thickness of the polymer layer is  $\approx$  4 nm for MSNs-NH<sub>2</sub>@PSPMK-0.125, 7 nm for MSNs-NH<sub>2</sub>@PSPMK-0.250, and 9 nm for MSNs-NH<sub>2</sub>@PSPMK-0.500, respectively, which indicates that there is a positive correlation between the SPMK monomer concentration and the polymer layer thickness.

Figure 1d exhibits the thermogravimetric analysis (TGA) results obtained for MSNs, MSNs-NH<sub>2</sub>, MSNs-NH<sub>2</sub>@I2959, and MSNs-NH<sub>2</sub>@PSPMK. To eliminate the interference from bound water on the surface of MSNs, the data are organized with the temperature starting from 100 °C. After amination and immobilization of the initiator, a weight loss of 12.9% and 14.2% is observed, through which the content of the initiator is calculated to be 1.5%. When the PSPMK polymer is grafted on the MSNs surface, the weight losses increase to 27.9% for MSNs-NH<sub>2</sub>@PSPMK-0.125, 29.1% for MSNs-NH<sub>2</sub>@PSPMK-0.250, and 38.0% for MSNs-NH<sub>2</sub>@PSPMK-0.500, respectively. As a result, the contents of the PSPMK polymer are calculated to be 16.0%, 17.4%, and 27.7%, respectively. The TGA data not only confirm the successful grafting of PSPMK polyelectrolyte polymer on the MSNs surface, but also provide a quantitative evaluation for each component of the nanoparticles, as summarized in Table 1. It can be observed that with increasing SPMK monomer concentration, the amount of the PSPMK polyelectrolyte polymer grafted on the MSNs surface increases remarkably.

**Table 1.** The weight ratio of each component in MSNs-NH<sub>2</sub>@I2959 and MSNs-NH<sub>2</sub>@PSPMK calculated from TGA data.

	MSNs-NH <sub>2</sub>	Irgacure 2959	PSPMK
MSNs-NH <sub>2</sub> @I2959	98.5%	1.5%	
MSNs-NH <sub>2</sub> @PSPMK-0.125	82.7%	1.3%	16.0%
MSNs-NH <sub>2</sub> @PSPMK-0.250	81.4%	1.2%	17.4%
MSNs-NH <sub>2</sub> @PSPMK-0.500	71.2%	1.1%	27.7%

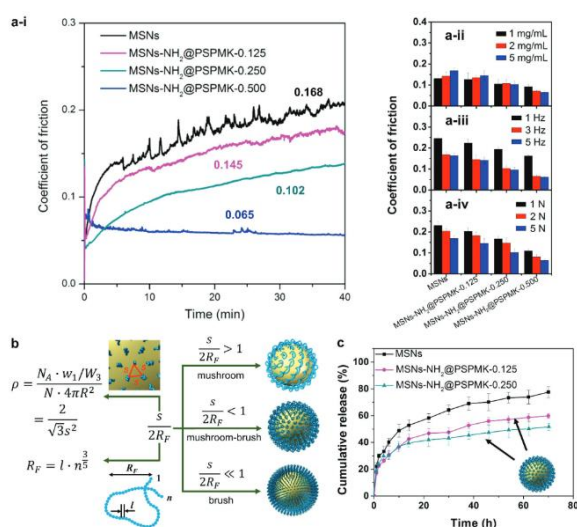
In order to further investigate the pore properties of MSNs and MSNs-NH<sub>2</sub>@PSPMK, the N<sub>2</sub> adsorption-desorption isotherms of the nanoparticles were measured. As shown in Figure 1e, all the isotherms demonstrate typical type IV N<sub>2</sub> adsorption/desorption patterns, indicating a mesoporous structure of the nanoparticles. Based on the Brunauer–Emmett–Teller (BET) model, the specific surface area and pore volume of MSNs are calculated to be 805 m<sup>2</sup> g<sup>-1</sup> and 0.806 mL g<sup>-1</sup>. Following grafting of PSPMK polyelectrolyte polymer on the MSNs surface, both specific surface area and pore volume of the nanoparticles decrease significantly, i.e., 429.6 m<sup>2</sup> g<sup>-1</sup> and 1.20 mL g<sup>-1</sup> for MSNs-NH<sub>2</sub>@PSPMK-0.125, 299.1 m<sup>2</sup> g<sup>-1</sup> and 1.11 mL g<sup>-1</sup> for MSNs-NH<sub>2</sub>@PSPMK-0.250 and 23.6 m<sup>2</sup> g<sup>-1</sup> and 0.09 mL g<sup>-1</sup> for MSNs-NH<sub>2</sub>@PSPMK-0.500, respectively. This result indicates that the mesoporous channels have been blocked by the PSPMK polyelectrolyte polymer.

Figure 1f displays the small-angle X-ray diffraction (XRD) patterns of MSNs and MSNs-NH<sub>2</sub>@PSPMK, showing the microcrystalline of the nanoparticles. The presence of the standard Bragg peaks of (100), (110), and (200) indicates the highly ordered hexagonal array of MSNs. After the MSNs surface is grafted with PSPMK polyelectrolyte polymer, the Bragg peaks of (110) and (200) almost disappear for all of the MSNs-NH<sub>2</sub>@PSPMK nanoparticles, which is

mainly due to the weak crystallinity of PSPMK polyelectrolyte polymer.

## 2.2 Superlubricated Property and Analysis

The tribological experiment was performed to investigate the lubrication property of MSNs and MSNs-NH<sub>2</sub>@PSPMK in aqueous suspension. As shown from the friction coefficient-time plots in Figure 2a-i (loading force: 5 N; reciprocating frequency: 3 Hz; concentration: 5 mg mL<sup>-1</sup>), the friction coefficient of MSNs is 0.168, which is much higher than that of MSNs-NH<sub>2</sub>@PSPMK with different monomer concentrations. Additionally, it is observed that as the monomer concentration increases, the friction coefficient value reduces gradually, i.e., 0.145 for MSNs-NH<sub>2</sub>@PSPMK-0.125, 0.102 for MSNs-NH<sub>2</sub>@PSPMK-0.250, and 0.065 for MSNs-NH<sub>2</sub>@PSPMK-0.500, respectively. Figure 2a-ii shows the comparison of friction coefficient lubricated using MSNs and MSNs-NH<sub>2</sub>@PSPMK at different aqueous suspension concentrations (1, 2, and 5 mg mL<sup>-1</sup>) under the reciprocating frequency of 3 Hz and the loading force of 5 N. It is observed that all the friction coefficients of MSNs-NH<sub>2</sub>@PSPMK are lower than that of MSNs, and generally the lubrication is improved with the increase in aqueous suspension concentration. Figure 2a-iii demonstrates the comparison of friction coefficient lubricated by MSNs and MSNs-NH<sub>2</sub>@PSPMK at different reciprocating frequencies (1, 3, and 5 Hz) under the loading force of 5 N and the aqueous suspension concentration of 5 mg mL<sup>-1</sup>. The friction coefficients are relatively small, and there seems to be a decreasing trend with the increase in reciprocating frequency although the difference between 3 and 5 Hz is slight. Figure 2a-iv presents the comparison of friction coefficient lubricated by MSNs and MSNs-NH<sub>2</sub>@PSPMK at different loading forces (1, 2, and 5 N) under the reciprocating frequency of 3 Hz and the aqueous suspension concentration of 5 mg mL<sup>-1</sup>. The friction coefficients remain at a low level, and there seems to be a decreasing trend with the increase in loading force. The results indicate that the charged polymer covering the surface of MSNs-NH<sub>2</sub>@PSPMK can achieve improved lubrication based on hydration lubrication mechanism,<sup>24</sup> which is mainly caused by the formation of hydration layers surrounding the negative charges of PSPMK polyelectrolyte polymer.



**Figure 2.** a-i) The lubrication property of MSNs and MSNs-NH<sub>2</sub>@PSPMK nanoparticles in aqueous suspension. Contacting pairs: Ti6Al4V disk and PE ball; duration: 40 min; oscillation amplitude: 4 mm; a-ii) aqueous suspension concentration: 1, 2, and 5 mg mL<sup>-1</sup>; a-iii) reciprocating frequency: 1, 3, and 5 Hz; a-iv) loading force: 1, 2, and 5 N. b) Schematic graph showing the calculation of different configurations of PSPMK polymer chains on the MSNs surface. The polymer chains are in the "mushroom-brush" state for MSNs-NH<sub>2</sub>@PSPMK-0.125 and MSNs-NH<sub>2</sub>@PSPMK-0.250, and they are in the "brush" state for MSNs-NH<sub>2</sub>@PSPMK-0.500. c) Release profiles of DS-loaded MSNs and DS-loaded MSNs-NH<sub>2</sub>@PSPMK nanoparticles in PBS at 37 °C for 72 h. A sustained drug release profile is observed for MSNs-NH<sub>2</sub>@PSPMK-0.125 and MSNs-NH<sub>2</sub>@PSPMK-0.250.

Figure 2a shows that the lubrication performance of MSNs-NH<sub>2</sub>@PSPMK improves significantly along with thicker PSPMK polymer layer on the MSNs surface. This phenomenon may be due to the different configurations of the PSPMK polymer chains, which exhibit three potential states, namely “mushroom” state (the polymer chains are aggregated), “mushroom-brush” state (the polymer chains are stretched incompletely), and “brush” state (the polymer chains are stretched completely) (Figure 2b), depending on the ratio of the average distance between the PSPMK polymer chains ( $s$ ) and the Flory radius ( $R_F$ ).<sup>25, 26</sup> Generally, in case that  $s$  is larger than  $2R_F$ , PSPMK polymer chains are in the “mushroom” state as a result of the free movement of polymer segments. If  $s$  is far less than  $2R_F$ , PSPMK polymer chains are in the “brush” state due to the repulsive force between the polymer chains. Besides, PSPMK polymer chains are in the “mushroom-brush” state. The values of  $s$  and  $R_F$  for MSNs-NH<sub>2</sub>@PSPMK with different SPMK monomer concentrations are calculated and summarized in Table 2, and the calculation process is mentioned in detail in the Supporting Information.

**Table 2.** Calculation of the parameters of PSPMK polymer chains for MSNs-NH<sub>2</sub>@PSPMK with different monomer concentrations.

	$n$	$R_F$ [nm]	$s$ [nm]	$s/2R_F$
MSNs-NH <sub>2</sub> @PSPMK-0.125	11.2	1.32	0.90	0.34
MSNs-NH <sub>2</sub> @PSPMK-0.250	13.2	1.46	0.90	0.31
MSNs-NH <sub>2</sub> @PSPMK-0.500	22.9	2.03	0.90	0.22

According to the previously published studies,<sup>19, 25</sup> when  $0.3 < s/2R_F < 1.2$ , the polymer chains can be generally considered in the “mushroom-brush” state (e.g., MSNs-NH<sub>2</sub>@PSPMK-0.125 and MSNs-NH<sub>2</sub>@PSPMK-0.250), and when  $s/2R_F < 0.3$ , the polymer chains will be in the “brush” state (e.g., MSNs-NH<sub>2</sub>@PSPMK-0.500). Figure 2a shows that the PSPMK polymer chains in the “mushroom-brush” state or “brush” state can result in a significant reduction in the friction coefficient. Additionally, the lubrication property of the PSPMK polymer chains in the “brush” state is even better than that in the “mushroom-brush” state, where the polymer chains are unable to be completely stretched out, and thus, hydration lubrication is to a certain degree compromised.

### 2.3 In Vitro Drug Loading and Release

The results of drug loading capacity (LC, %) and encapsulation efficiency (EE, %) of MSNs and MSNs-NH<sub>2</sub>@PSPMK are shown in Table 3.

**Table 3.** Loading capacity (LC, %) and encapsulation efficiency (EE, %) of DS-loaded MSNs and DS-loaded MSNs-NH<sub>2</sub>@PSPMK.

	LC [%]	EE [%]
MSNs	5.8	77.2
MSNs-NH <sub>2</sub> @PSPMK-0.125	2.8	36.4
MSNs-NH <sub>2</sub> @PSPMK-0.250	2.3	29.6
MSNs-NH <sub>2</sub> @PSPMK-0.500	0.4	4.9

The PSPMK polyelectrolyte polymer on the MSNs surface impedes encapsulation of DS, and MSNs-NH<sub>2</sub>@PSPMK-0.500 hardly adsorb any DS, indicating that the polymer layer is too thick for the drug molecules to penetrate through into the channels. Figure 2c presents the release profiles of DS-loaded MSNs and DS-loaded MSNs-NH<sub>2</sub>@PSPMK. All the curves show an initial rapid drug release within 10 h, followed by a relatively flat stage afterward. When MSNs, MSNs-NH<sub>2</sub>@PSPMK-0.125, and MSNs-NH<sub>2</sub>@PSPMK-0.250 are used as the nanocarriers, 77.6%, 59.8%, and 47.2% of DS are released within 72 h, respectively, demonstrating the excellent sustained release effect of MSNs-NH<sub>2</sub>@PSPMK. It is noted that the release profile of MSNs-NH<sub>2</sub>@PSPMK-0.500 is not provided due to the extremely low drug loading capacity.

From Table 3 it can be seen that the drug loading capacity of MSNs-NH<sub>2</sub>@PSPMK decreases along with thicker PSPMK polymer layers on the MSNs surface. Additionally, from the drug release profiles of the three nanoparticles in Figure 2c, MSNs-NH<sub>2</sub>@PSPMK-0.125 and MSNs-NH<sub>2</sub>@PSPMK-0.250 exhibit a sustained drug release behavior, indicating that the hydrated PSPMK polymer chains on the MSNs surface are both penetrable and impeditive for the drug. It is considered that when the polymer chains are in the “mushroom-brush” state or the short-length “brush” state, MSNs-NH<sub>2</sub>@PSPMK can be used as a nanocarrier for sustained drug release, until the length of the polymer chains increases and blocks drug loading into the mesoporous channels of the nanoparticles, e.g., in the case of MSNs-NH<sub>2</sub>@PSPMK-0.500. In addition, the drug loading process of MSNs-NH<sub>2</sub>@PSPMK, i.e., the preparation of DS-loaded MSNs-NH<sub>2</sub>@PSPMK, is performed after surface grafting of PSPMK polyelectrolyte polymer on the MSNs surface. This is mainly because the drug may experience a rapid release during the photopolymerization process if it is initially loaded into MSNs. On the other hand, the UV-irradiation may cause potential influence on the drug activity, which as a consequence further affects the therapeutic effect of DS-loaded MSNs-NH<sub>2</sub>@PSPMK for oxidative stress-induced degeneration of chondrocytes (in vitro test) and treatment of osteoarthritis (in vivo test).

## 2.4 In Vitro Cytotoxicity and Protective Effect of Chondrocytes

### Degeneration

In order to examine the potential clinical application of the developed superlubricated drug-loaded

nanoparticles, we investigated the in vitro cytotoxicity of MSNs, MSNs-NH<sub>2</sub>@PSPMK, and MSNs-NH<sub>2</sub>@PSPMK-DS on primary rat chondrocytes, and subsequently performed experiments to indicate whether MSNs-NH<sub>2</sub>@PSPMK-DS could protect the oxidative stress-induced degeneration of the chondrocytes. It was noted that MSNs-NH<sub>2</sub>@PSPMK and MSNs-NH<sub>2</sub>@PSPMK-DS used in the following tests were prepared with the SPMK monomer concentration of 0.250 m, as the nanoparticles made at this concentration demonstrated both good lubrication property and sustained drug release behavior.

The in vitro cytotoxicity of MSNs, MSNs-NH<sub>2</sub>@PSPMK, and MSNs-NH<sub>2</sub>@PSPMK-DS on primary rat chondrocytes are first discussed. Following incubation at 1, 3, and 5 d, the cells were proceeded for CCK-8 test and Live/Dead assay. In Figure 3a the CCK-8 test shows that the cell viability and proliferation activity have no significant difference among the experimental groups compared with the control group at all time points. In addition, the Live/Dead staining show that most of the seeded cells stay alive and only very few dead cells are observed over the course of 5-d culture (Figure 3b). Furthermore, the cell density increased gradually with time from day 1 to day 5, which is confirmed by the data of the number of viable cells shown in Figure 3c. All these results indicate that the nanoparticles show excellent biocompatibility to the chondrocytes.

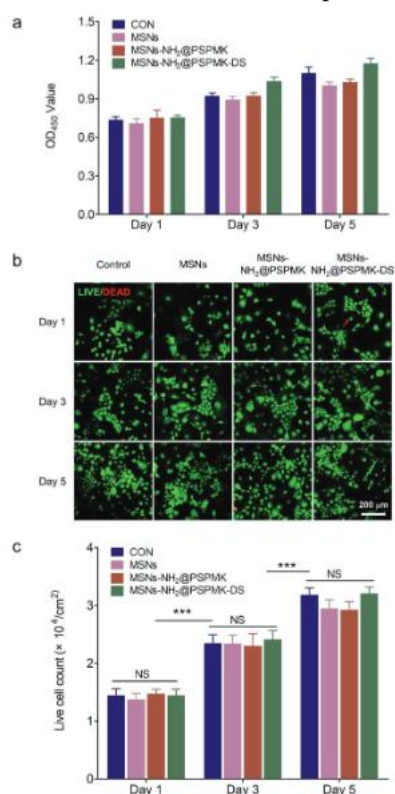


**Figure 3.** a) Cytotoxicity of MSNs, MSNs-NH<sub>2</sub>@PSPMK, and MSNs-NH<sub>2</sub>@PSPMK-DS on chondrocytes examined with CCK-8. b) Live/Dead staining of chondrocytes co-cultured with MSNs, MSNs-NH<sub>2</sub>@PSPMK, and MSNs-NH<sub>2</sub>@PSPMK-DS detected employing fluorescence microscopy. All the nanoparticles show excellent biocompatibility to the chondrocytes. c) The live cell count summarized from the Live/Dead assay. *n* = 3; NS = no significance; \*\*\**P* < 0.001.

Multiple factors are associated with pathogenesis of osteoarthritis, such as reactive oxygen species (ROS), mechanical loading stress, and inflammatory factors. These factors can result in chondrocytes degeneration, which is the most significant characteristic of osteoarthritis. In this study, we introduced H<sub>2</sub>O<sub>2</sub> to simulate ROS stress of chondrocytes during the pathogenesis of

osteoarthritis. The robust production of Col2 $\alpha$  and aggrecan are important characteristics of healthy chondrocytes. After addition of H<sub>2</sub>O<sub>2</sub>, the mRNA expression of Col2 $\alpha$  and aggrecan both decrease gradually with prolonged culture time and to less than half of the original value (0 h) at 12 h. Moreover, a significant reduction in the mRNA expression of Col2 $\alpha$  and aggrecan is observed at 24 h after addition of H<sub>2</sub>O<sub>2</sub> (Figure 4a,b). In order to explore the protective effect of MSNs-NH<sub>2</sub>@PSPMK-DS for chondrocytes degeneration, subsequently we evaluated the mRNA expression of Col2 $\alpha$  and aggrecan in chondrocytes after addition of MSNs, MSNs-NH<sub>2</sub>@PSPMK, and MSNs-NH<sub>2</sub>@PSPMK-DS with H<sub>2</sub>O<sub>2</sub>. The qRT-PCR analyses indicate that the mRNA expression of Col2 $\alpha$  and aggrecan increases significantly after addition of MSNs-NH<sub>2</sub>@PSPMK-DS, whilst no significant changes have been observed for MSNs and MSNs-NH<sub>2</sub>@PSPMK, which clearly indicates the protective effect of MSNs-NH<sub>2</sub>@PSPMK-DS for chondrocytes degeneration (Figure 4c,d).

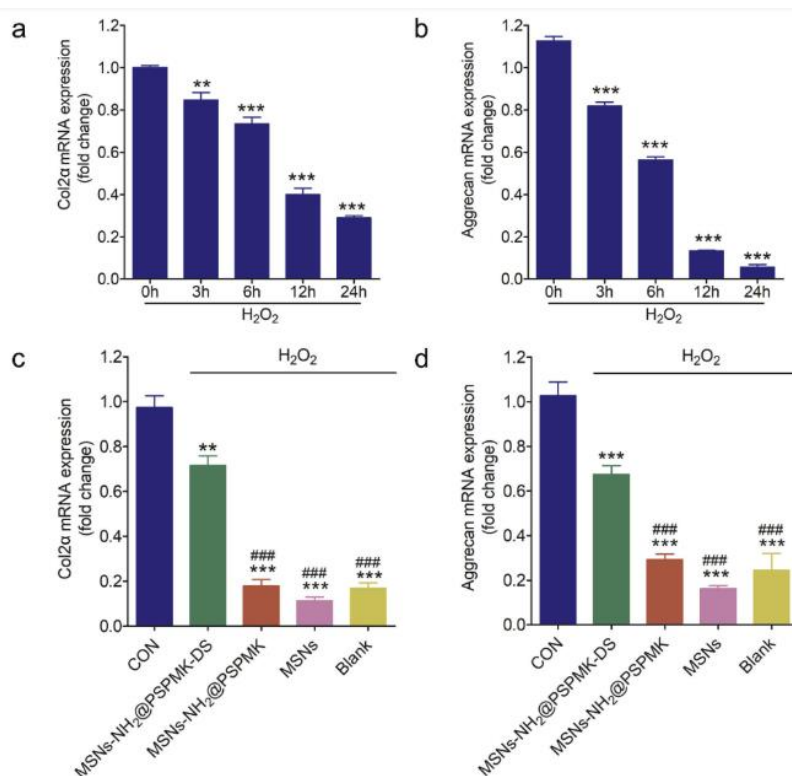


**Figure 4.** a,b) The qRT-PCR analysis exhibiting the mRNA expression of a) Col2 $\alpha$  and b) aggrecan in chondrocytes treated with 10  $\mu$ M of H<sub>2</sub>O<sub>2</sub> at different time points.  $n = 3$ , \* $P < 0.05$ , \*\* $P < 0.01$ , \*\*\* $P < 0.001$ , compared with control (0 h). c,d) The qRT-PCR analysis showing the mRNA expression of c) Col2 $\alpha$  and d) aggrecan in chondrocytes treated with 10  $\mu$ M of H<sub>2</sub>O<sub>2</sub>, and cocultured with MSNs, MSNs-NH<sub>2</sub>@PSPMK, and MSNs-NH<sub>2</sub>@PSPMK-DS for 24 h.  $n = 3$ , \*\* $P < 0.01$ , \*\*\* $P < 0.001$ , compared with control; ### $P < 0.001$ , compared with MSNs-NH<sub>2</sub>@PSPMK-DS. The data clearly demonstrate the protective effect of MSNs-NH<sub>2</sub>@PSPMK-DS for chondrocytes degeneration.

Furthermore, the result of immunofluorescence staining and corresponding statistical analysis show that the addition of MSNs-NH<sub>2</sub>@PSPMK-DS can reverse H<sub>2</sub>O<sub>2</sub> stress-induced reduction of Col2 $\alpha$  protein expression compared with the MSNs and MSNs-NH<sub>2</sub>@PSPMK groups (Figure 5). As a consequence, the results confirm the protective effect of MSNs-NH<sub>2</sub>@PSPMK-DS for chondrocytes degeneration and tentatively suggest the potential clinical application for treatment of osteoarthritis.

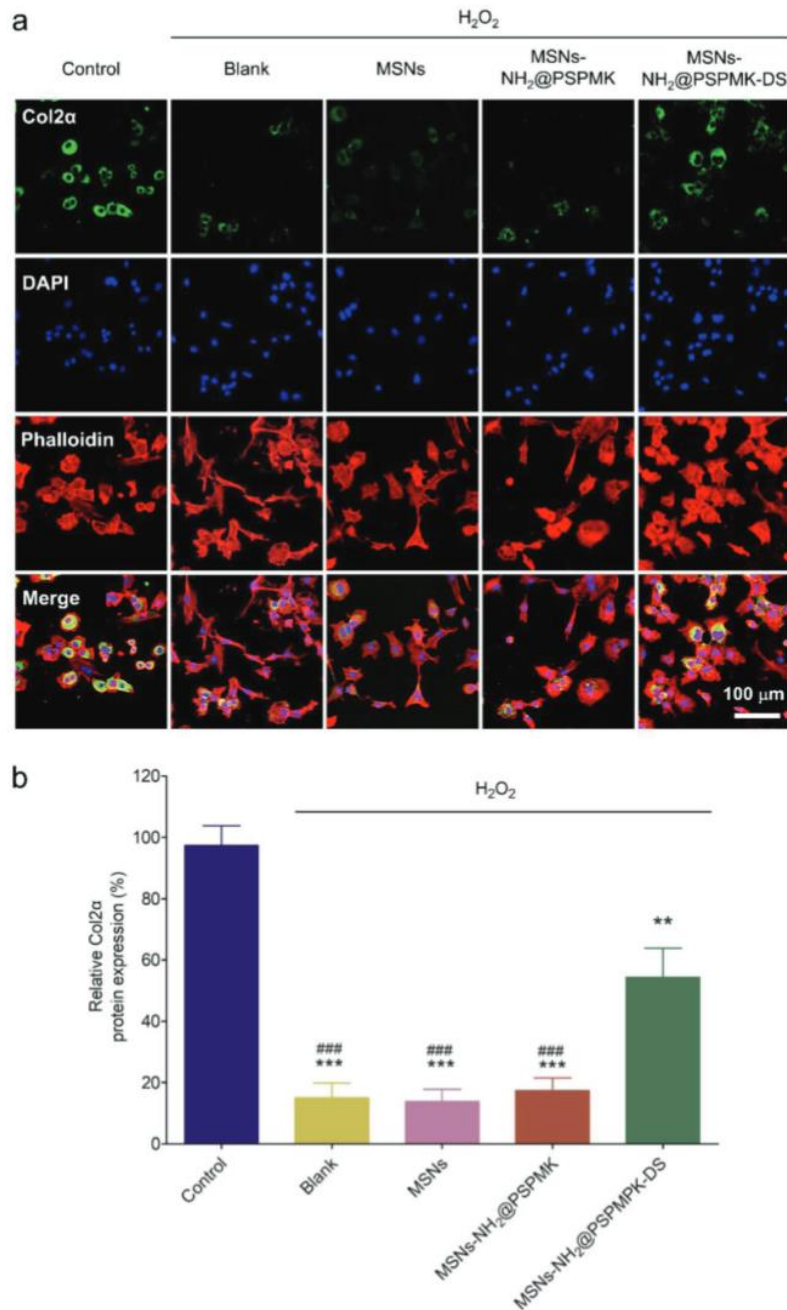


**Figure 5.** a) Representative photomicrographs of chondrocytes treated with 10  $\mu$ M of H<sub>2</sub>O<sub>2</sub> and co-cultured with MSNs, MSNs-NH<sub>2</sub>@PSPMK, and MSNs-NH<sub>2</sub>@PSPMK-DS for 12 h, acquired using a laser scanning confocal microscopy. Green: Molecular Probes labeling Col2 $\alpha$ ; blue: DAPI labeling cell nuclei; red: Phalloidin labeling cell actin. b) The quantitative data showing comparison of Col2 $\alpha$  protein expression of chondrocytes treated with 10  $\mu$ M of H<sub>2</sub>O<sub>2</sub>, and co-cultured with MSNs, MSNs-NH<sub>2</sub>@PSPMK, and MSNs-NH<sub>2</sub>@PSPMK-DS for 12 h.  $n = 3$ ,  $^{**}p < 0.01$ ,  $^{***}p < 0.001$ , compared with control;  $^{###}p < 0.001$ , compared with MSNs-NH<sub>2</sub>@PSPMK-DS. The results confirm the protective effect of MSNs-NH<sub>2</sub>@PSPMK-DS for chondrocytes degeneration.

## 2.5 In Vitro Therapeutic Effect of Osteoarthritis

An animal model of destabilization of the medial meniscus (DMM)-induced osteoarthritis has been commonly employed in previous studies.<sup>27</sup> In the present study, we performed in vivo analysis of Sprague-Dawley rats that had undergone DMM surgery, including X-ray radiograph and histological staining. One week following the DMM surgery, the rats were injected once every week with phosphate buffer solution (PBS), MSNs, MSNs-NH<sub>2</sub>@PSPMK, and MSNs-NH<sub>2</sub>@PSPMK-DS. Figure 6a shows the X-ray radiographs of the knee joints of the rats

obtained at one and eight weeks after the DMM surgery, and no signs of acute inflammation are observed in any of these treatment groups (including MSNs, MSNs-NH<sub>2</sub>@PSPMK, and MSNs-NH<sub>2</sub>@PSPMK-DS). In addition, the values of articular space width are calculated from the radiographies, and it is indicated that the medial compartments between femur and tibia become narrower at eight weeks after DMM surgery for all the groups, although it seems that the MSNs-NH<sub>2</sub>@PSPMK-DS group generates a slightly larger articular space width, Figure 6b.

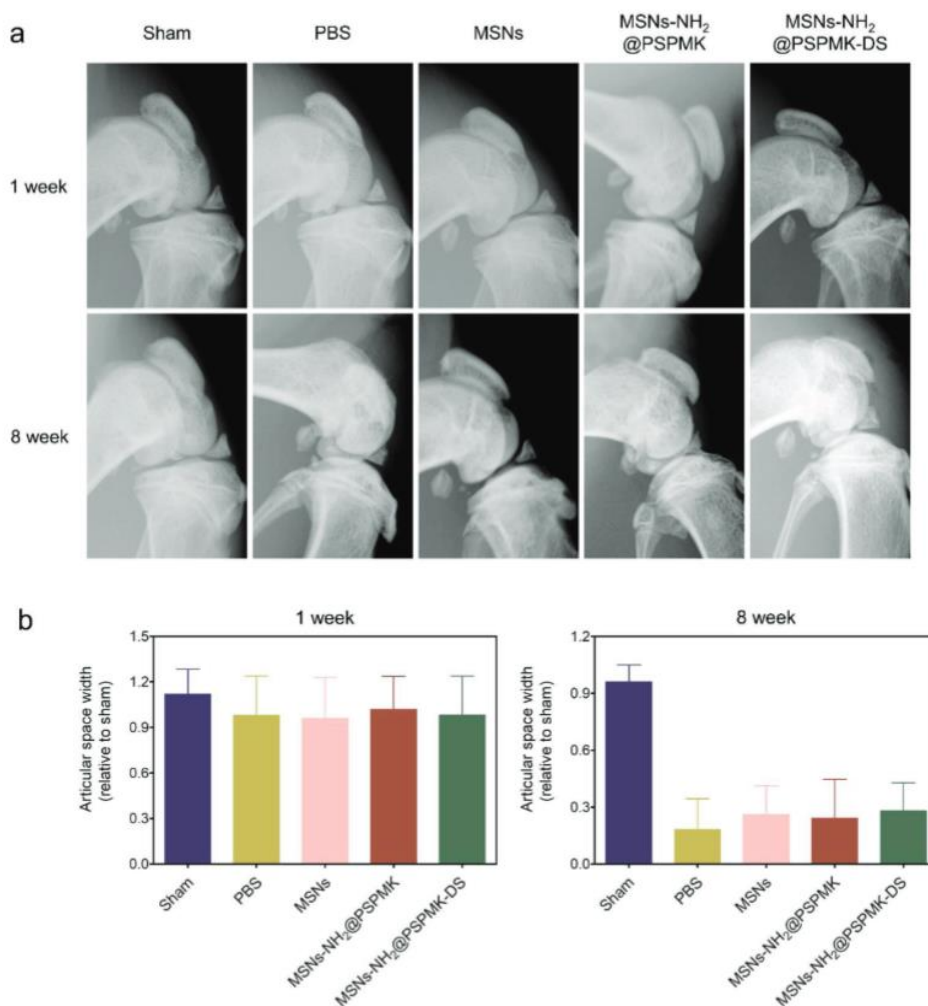


**Figure 6.** a) Representative X-ray radiographs of the rat knee joints showing the intra-articular injection of PBS, MSNs, MSNs-NH<sub>2</sub>@PSPMK, and MSNs-NH<sub>2</sub>@PSPMK-DS in the treatment of DMM-induced osteoarthritis at one and eight weeks after surgery. b) The relative articular space width between the medial compartments of rat knee joints at one and eight weeks after surgery. No signs of acute inflammation are observed from the X-ray radiographies of the MSNs, MSNs-NH<sub>2</sub>@PSPMK, and MSNs-NH<sub>2</sub>@PSPMK-DS groups.

The cartilage tissues were then evaluated histologically by hematoxylin-eosin (H&E) staining and Safranin O-fast green staining. As displayed in Figure 7a,b, typical osteoarthritis features, such as surface discontinuity, vertical fissure, erosion denudation and deformation, are observed in the PBS group. Compared with the PBS group, all the treatment groups present varied degrees of improvement with respect to morphological change, matrix staining and tidemark integrity promotion. Specifically, the MSNs-NH<sub>2</sub>@PSPMK-DS group is considered the most effective in maintaining the columnar architecture of normal cartilage, which is typically manifested as less severe lesion and extensive erosion, decreased surface denudation and deformation, as well as increased tissue cellularity and cloning. Furthermore, the MSNs-NH<sub>2</sub>@PSPMK-DS group shows

more intense Safranin O-fast green positive staining than do the other groups (Figure 7c). This finding indicates that the MSNs-NH<sub>2</sub>@PSPMK-DS group has better outcome with respect to glycosaminoglycan deposition, attenuation of cartilage matrix depletion and also retention of overall cartilage thickness. The result of OARSI score is illustrated in Figure 7d. All the treatment groups decrease the OARSI score more or less compared with the PBS group, and the MSNs-NH<sub>2</sub>@PSPMK-DS group shows the best result with about 64% reduction. In addition, the depth of the cartilage macroscopic lesion is also compared for each group at eight weeks after DMM surgery, and again the MSNs-NH<sub>2</sub>@PSPMK-DS group demonstrates the best result with about 55% reduction relative to the PBS group (Figure 7e). All these results indicate that the superlubricated drug nanocarrier (MSNs-NH<sub>2</sub>@PSPMK-DS) can inhibit development of osteoarthritis based on the in vivo rat DMM model.

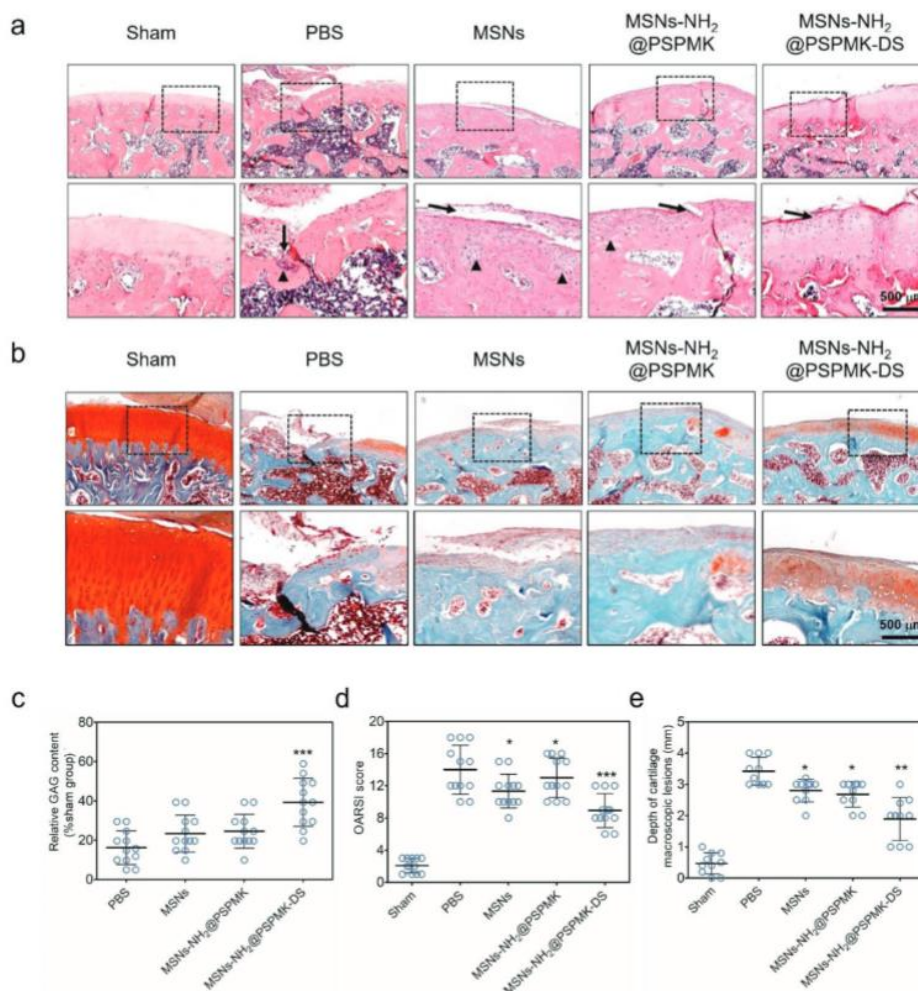


**Figure 7.** a) Representative H&E staining and b) Safranin O-fast green staining of the cartilage sections after treatment of rat DMM-induced osteoarthritis employing PBS, MSNs, MSNs-NH<sub>2</sub>@PSPMK, and MSNs-NH<sub>2</sub>@PSPMK-DS at eight weeks after surgery. Extensive morphological and cellular changes in the PBS group are reflected by surface irregularities and fissures (black arrows), increase in tissue cellularity with cloning (black triangles), along with full-depth erosion and widespread cell loss. The MSNs-NH<sub>2</sub>@PSPMK-DS group presents the best result in maintaining columnar architecture of normal cartilage. c) Glycosaminoglycan (GAG) content relative to the sham group obtained from the quantification of Safranin O-fast green staining of the cartilage sections using the Image J software. The values are presented as mean  $\pm$  SD,  $n = 12$ . d) OARSI score of articular cartilage for each group after treatment for eight weeks. The values are presented as mean  $\pm$  SD,  $n = 12$ . e) Depth of cartilage macroscopic lesion for each group after treatment for eight weeks. The values are presented as mean  $\pm$  SD,  $n = 10$ . \* $P < 0.05$ , \*\* $P < 0.01$ , \*\*\* $P < 0.001$ , compared with the PBS group. The results of (c)–(e) indicate that the MSNs-NH<sub>2</sub>@PSPMK-DS group with enhanced lubrication and sustained drug release, which is bioinspired by the structure of fresh *Euryale ferox* seed, demonstrates the best therapeutic effect in the treatment of osteoarthritis based on the rat DMM model.

### 3 Conclusions

In the present study, inspired by the fresh euryale ferox seed, we introduced a facile and low-toxic photopolymerization method and successfully synthesized PSPMK polymer brushes-grafted MSNs (MSNs-NH<sub>2</sub>@PSPMK), which with a controllable state of the polymer chains, acted as novel nanoparticles for efficient lubrication and sustained drug release. Such nanoparticles were then encapsulated with DS to prepare the superlubricated drug-loaded nanoparticles, MSNs-NH<sub>2</sub>@PSPMK-DS, for the treatment of osteoarthritis. The lubrication and drug release tests revealed that the lubrication capability of the developed nanoparticles could be improved, while the drug release rate be sustained with the increase in the thickness of the PSPMK polymer layer. The in vitro and in vivo experiments showed that the superlubricated drug-loaded nanoparticles with excellent biocompatibility not only protected the chondrocytes from oxidative stress-induced degeneration, but also provided therapeutic effect against development of osteoarthritis based on a rat DMM model. Combing the advantage of both efficient lubrication capability and drug loading and release behavior, the superlubricated drug-loaded nanoparticles, MSNs-NH<sub>2</sub>@PSPMK-DS, developed here are considered to have great potential for various biomedical applications, particularly in the situations where these two typical features are preferably desirable, for example, the treatment of osteoarthritis.

## 4 Experimental Section

Preparation of MSNs and MSNs-NH<sub>2</sub>: MSNs were prepared with reference to our previous studies.<sup>28-31</sup> Briefly, 0.5 g of cetyltrimethyl ammonium bromide (CTAB, 98%) and 1.75 mL of NaOH solution (2 m) were added to 240 mL of aqueous solution under stirring. Afterward, 5 mL of tetraethyl orthosilicate (TEOS, 98%) was added, and then the solution was vigorously stirred at 80 °C for 15 min, followed by normal stirring for 6 h. The solution was filtered and washed with deionized water and methanol, and the CTAB template was extracted by stirring in 50 mL of methanol and 5 mL of concentrated hydrochloric acid at 60 °C for 24 h. The final resulting product (MSNs) was filtered and washed with methanol and dried under vacuum.

In order to prepare amino MSNs (MSNs-NH<sub>2</sub>), 500 mg of MSNs was dispersed in 50 mL of anhydrous toluene, and 5 mL of 3-aminopropyltriethoxysilane (APTES, 98%) was added. The solution was refluxed under a nitrogen atmosphere for 24 h. The resulting product (MSNs-NH<sub>2</sub>) was collected through centrifugation (8000 rpm, 10 min), washed twice with toluene and ethanol and dried under vacuum.

Synthesis of Photopolymerization Initiator: Photopolymerization initiator was synthesized following the previously published protocol.<sup>32</sup> 2-hydroxy-1-[4-(2-hydroxyethoxy)phenyl]-2-methyl-1-propanone (Irgacure 2959, 26.9 g, 0.12 mol), p-methyl benzene sulfonic chloride (TsCl, 19.0 g, 0.10 mol), and KOH (22.4 g, 0.40 mol) were dissolved in 300 mL of CH<sub>2</sub>Cl<sub>2</sub> in a three-necked round bottom flask. The solution was stirred at room temperature for 2 h and then washed three times with deionized water. The organic layer was dried over Na<sub>2</sub>SO<sub>4</sub> and distilled under vacuum. The resulting product was purified using silica gel (200–300 mesh) column chromatography, with ethyl acetate and methylene chloride (1:4, v/v) as an elution. The final product was named as 2959-Tos.

Immobilization of 2959-Tos onto MSNs-NH<sub>2</sub>: Briefly, 2959-Tos (1 g), MSNs-NH<sub>2</sub> (400 mg), and K<sub>2</sub>CO<sub>3</sub> (2 g) were dissolved in 30 mL of N,N-dimethylformamide (DMF, 99%) in a 50 mL round bottom flask. The solution was stirred at 110 °C for 24 h. The resulting product (MSNs-NH<sub>2</sub>@I2959) was collected by centrifugation (8000 rpm, 15 min), washed with DMF and deionized water for several times, and finally dried under vacuum at room temperature overnight.

Synthesis of MSNs-NH<sub>2</sub>@PSPMK: MSNs-NH<sub>2</sub>@I2959 (100 mg) and SPMK monomer (1.25, 2.50, and 5.00 mmol) were dispersed in 10 mL of deionized water in a 50 mL round bottom flask. The mixture was deoxygenated by bubbling nitrogen for 30 min, and then photopolymerization was processed at 80 °C under UV-irradiation with an intensity of 5 mW cm<sup>-2</sup> for 90 min. The resulting product (MSNs-NH<sub>2</sub>@PSPMK) was collected through centrifugation, washed with ethanol/H<sub>2</sub>O (1:1, v/v) for several times, and finally dried under vacuum overnight. The product was distinguished by the monomer concentration used during the photopolymerization reaction, i.e., MSNs-NH<sub>2</sub>@PSPMK-0.125 (0.125 m SPMK), MSNs-NH<sub>2</sub>@PSPMK-0.250 (0.250 m SPMK), and MSNs-NH<sub>2</sub>@PSPMK-0.500 (0.500 m SPMK).

Characterization: FTIR spectrum was recorded employing a Nicolet 6700 transform infrared spectrometer (Thermo Scientific, USA) at a wavelength ranging from 400 cm<sup>-1</sup> to 4000 cm<sup>-1</sup>. XPS spectrum was recorded using a 250XI XPS system (Thermo Scientific, USA), and the binding energy data were calibrated against O1s peak at 523 eV. TGA was performed on a Q5000IR instrument (TA Instruments, USA). Field emission TEM (FEI, JEM-2100F, JEOL, Japan) was used to observe the morphologies of MSNs and MSNs-NH<sub>2</sub>@PSPMK. BET model was used to calculate specific surface area and pore volume of MSNs and MSNs-NH<sub>2</sub>@PSPMK on the basis of the adsorption data obtained by a NOVA4000 nitrogen adsorption instrument (Quantachrome Instruments, USA). Small angle XRD measurement was performed using a diffractometer (D8, Bruker, USA) over a 2θ range from 0.6° to 10° at a scanning speed of 1° min<sup>-1</sup>.

Lubrication Property: The tribological experiment was performed employing a universal material tester (UMT-3, Centre for Tribology Inc., Campbell, California, USA). All the tests were done in a reciprocating mode (oscillation amplitude: 4 mm; reciprocating frequency: 1 Hz, 3 Hz and 5 Hz) for a duration of 40 min, and the loading force was set at 1, 2, and 5 N. A polished Ti6Al4V disk with a surface roughness of 1.7 nm was employed as the lower specimen, and a polyethylene (PE) ball (diameter: 8 mm) was used as the upper specimen. Here, Ti6Al4V disk and PE ball were chosen as the specimens as they have been considered to represent the most typical biomaterials for total joint replacement prosthesis, and consequently can be used to mimic physiological conditions in the joint. Different concentrations (1 mg mL<sup>-1</sup>, 2 mg mL<sup>-1</sup> and 5 mg mL<sup>-1</sup>) of MSNs or MSNs-NH<sub>2</sub>@PSPMK aqueous suspension were added between the two contacting pairs as the lubricant. The apparent maximum contact pressure was calculated using the Hertz equation based on the ball-on-flat configuration from the previous studies (Equation 1),<sup>33-36</sup> where P is the apparent maximum contact pressure, F is the loading force (1, 2, and 5 N), R is the radius of the PE ball (4 mm), E<sub>1</sub> and μ<sub>1</sub> are the elastic modulus and Poisson's ratio of Ti6Al4V (110 GPa, 0.3), and E<sub>2</sub> and μ<sub>2</sub> are the elastic modulus and Poisson's ratio of PE (1 GPa, 0.4). Accordingly, the apparent maximum contact pressures were calculated to be 26.0 MPa (1 N), 32.0 MPa (2 N), and

43.8 MPa (5 N), respectively

$$P = \frac{1}{\pi} \sqrt[3]{\frac{6F}{\left(\frac{1-\mu_1^2}{E_1} + \frac{1-\mu_2^2}{E_2}\right)^2 R^2}}$$

(1)

**In Vitro Drug Loading and Release:** In order to load the drug, MSNs (20 mg) and SNs-NH<sub>2</sub>@PSPMK (20 mg) were added to 10 mL of DS solution (0.5 × 10<sup>-3</sup> m) in PBS (pH 7.4). The nanoparticles were uniformly dispersed by ultrasound, and then the mixture was stirred for 48 h. The DS-loaded nanoparticles were collected by centrifugation, washed with deionized water for several times, and finally dried under vacuum. The amount of DS remaining in the solution was analyzed by a UV-vis spectrophotometer (UV-6100s, Metash Instruments, China) at a wavelength of 276 nm. The relationship between DS concentration in PBS and its absorbance at the wavelength of 276 nm was measured beforehand as the reference. The drug loading capacity (LC, %) and encapsulation efficiency (EE, %) were calculated by Equations 2–4

$$LC (\%)_{\text{MSNs}} = \frac{\text{amount of loaded DS}}{\text{amount of DS-loaded MSNs}} \times 100$$

(2)

$$LC (\%)_{\text{MSNs-NH}_2@ \text{PSPMK}} = \frac{\text{amount of loaded DS}}{\text{amount of DS-loaded MSNs-NH}_2@ \text{PSPMK}} \times 100$$

(3)

$$EE(\%) = \frac{\text{amount of loaded DS}}{\text{amount of added DS}} \times 100$$

(4)

Subsequently, 20 mg of DS-loaded MSNs and 20 mg of DS-loaded MSNs-NH<sub>2</sub>@PSPMK were first uniformly dispersed in 10 mL of PBS, respectively, and then 2 mL of each sample was put into dialysis tubes (molecular weight cutoff: 8000–10 000). The tubes were dialyzed in 20 mL of PBS at 37 °C. After a predetermined time, 2 mL of the medium was taken out from the release buffer and replaced by 2 mL of fresh PBS. Finally, the amount of DS released from DS-loaded nanoparticles was evaluated by the UV-vis spectrophotometer.

**Primary Rat Chondrocytes Isolation:** Chondrocytes were isolated from the articular cartilage of rats in the knee joint as previously reported.<sup>37</sup> The articular cartilage tissues were cut into small pieces (1 mm<sup>3</sup>) and digested with 0.25% trypsin for 30 min, followed by digestion with 0.2% type

II collagenase for 4 h. The released cells were then cultured in DMEM/F12 media supplemented with 10% fetal bovine serum and antibiotics. Only the cells with less than three passages were used in this study in order to preserve the chondrocytes' phenotype. Unless otherwise explained, the MSNs-NH<sub>2</sub>@PSPMK and MSNs-NH<sub>2</sub>@PSPMK-DS used in the following tests were prepared with the SPMK monomer concentration of 0.250 m.

**Cell Cytotoxicity:** The primary rat chondrocytes were seeded in 24-well plates with a cell density of  $5 \times 10^4$  mL<sup>-1</sup>. The plates were incubated in a humidified atmosphere at 37 °C and 5% CO<sub>2</sub>, and the culture medium of the plates was replaced every other day. After treatment with 1 mg mL<sup>-1</sup> of MSNs, MSNs-NH<sub>2</sub>@PSPMK, and MSNs-NH<sub>2</sub>@PSPMK-DS in triplicate for 1, 3, and 5 d, the Cell Counting Kit-8 (CCK-8, Dojindo Kagaku, Japan) was used to investigate the cytotoxicity of the nanoparticles on chondrocytes. Briefly, 0.5 mL of fresh culture medium and 50 μL of CCK-8 solution were added to each well of the plates. After incubation for 2 h, the mixed medium was transferred to 96-well plates in the darkness. The absorbance of the solution was measured employing a microplate reader (Infinite F50, Tecan, Switzerland) at a wavelength of 450 nm.

**Live/Dead Staining:** The cell viability of the nanoparticles was analyzed by a Live/Dead Cell kit (Life Tech, USA). Chondrocytes were seeded and cultured the same as before. After being cocultured with 1 mg mL<sup>-1</sup> of MSNs, MSNs-NH<sub>2</sub>@PSPMK, and MSNs-NH<sub>2</sub>@PSPMK-DS in triplicate for 1, 3, and 5 d, the cells were stained with 500 μL of Live/Dead cell dye for 15 min, and observed employing a fluorescence microscopy (ZEISS, Axio Imager M1, Germany). As described in the manufacturer's protocol, the viable cells with esterase activity appeared green, whereas the dead cells with compromised plasma membranes appeared red.

**qRT-PCR Analysis:** The primary rat chondrocytes were seeded in 6-well plates with a cell density of  $5 \times 10^5$  mL<sup>-1</sup>, treated with 10 mU of H<sub>2</sub>O<sub>2</sub> and cocultured with 1 mg mL<sup>-1</sup> of MSNs, MSNs-NH<sub>2</sub>@PSPMK, and MSNs-NH<sub>2</sub>@PSPMK-DS for 24 h. Total RNA from chondrocytes was extracted using TRIzol reagent (Invitrogen, USA) based on previously reported study.<sup>38</sup> The concentration and purity of the RNA preparations were determined through measuring the absorbance of RNA at 260 and 280 nm. cDNA was synthesized using 1 μg of RNA and a RevertAid First Strand cDNA Synthesis Kit (TaKaRa, Dalian, China). Quantitative real-time polymerase chain reaction (qRT-PCR) was performed to amplify the cDNA employing the SYBR Premix Ex Tag Kit (TaKaRa) and an ABI 7500 sequencing detection system (Applied Biosystems, Foster City, CA, USA). The mRNA levels of collagen II (Col2<sup>α</sup>), aggrecan, and GAPDH were quantified by using specific primers and normalized to GAPDH. The primer sequences used in this study were as follows: GAPDH: forward, 5' -GAAGTTCGGTGTGAACGGATTTG-3' ; reverse, 5' -CATGTAGA-CCATGTAGTTGAGGTCA-3' ; Col2<sup>α</sup> : forward, 5' -CTCAAGTCGCTGAA-CAACCA-3' ; reverse, 5' -GTCTCCGCTCTTCCACTCTG-3' ; aggrecan: forward, 5' -GATCTCAGTGGGCAACCTTC-3' ; reverse, 5' -TCCACAAACGTAATG-CCAGA-3' .

**Immunofluorescence Staining:** The chondrocytes were seeded onto sterile cover slips at a density of  $5 \times 10^4$  cells per well in 24-well culture plates, treated with 10 mU of H<sub>2</sub>O<sub>2</sub> and cocultured

with 1 mg mL<sup>-1</sup> of MSNs, MSNs-NH<sub>2</sub>@PSPMK, and MSNs-NH<sub>2</sub>@PSPMK-DS. After incubation for 12 h, the cells were fixed in 4% paraformaldehyde for 10 min, treated with 0.1% Triton X-100 for 15 min, and incubated in 3% bovine serum albumin (BSA)/PBS for 30 min at room temperature. Afterward, the cells were incubated with rat anti-Col2 $\alpha$  antibody (1:200 dilution) at 4 °C overnight. Following primary antibody incubation, the cells were washed employing PBS and incubated with appropriate Alexa Fluor-coupled secondary antibodies (Molecular Probes, Life Tech, USA, 1:400) for 1 h at room temperature. The cell nuclei were counterstained with 4, 6-diamidino-2-phenylindole diacetate (DAPI, Life Tech, USA) at room temperature for 15 min in the darkness. Additionally, the cell actin was labeled with Alexa Fluor 594 phalloidin (Life Tech, USA). The images were acquired using a laser scanning confocal microscopy (LSCM, LSM800, ZEISS, Germany).

**Rat Osteoarthritis Model and Surgical Procedure:** This animal experiment was approved by the Animal Research Committee of Ruijin Hospital, School of Medicine, Shanghai Jiaotong University, China, which was in compliance with the National Institutes of Health Guidelines for the Care and Use of Laboratory Animals. An osteoarthritis model was established via DMM surgery in male Sprague-Dawley rats (12 weeks old; n = 25; mean body weight: 256.7 g). After the rats were anesthetized by intraperitoneal injection of pentobarbital sodium (30 mg kg<sup>-1</sup> body weight), the right knee joint was exposed following a medial capsular incision and gentle lateral displacement of the extensor muscles without transection of the patellar ligament. Afterward, the medial meniscus ligament (MML) was transected and then the medial meniscus could be removed medially. The medial capsular incision was well sutured after restoring the extensor muscles. Additionally, a sham operation was performed employing the same approach without MML transection. The rats were then permitted unrestricted activity and provided free access to food and water. One week after the surgical operation, the rats were randomly sorted into five groups (n = 5 for each group) and intra-articularly injected once every week with the following formulations, i.e., PBS, MSNs, MSNs-NH<sub>2</sub>@PSPMK, and MSNs-NH<sub>2</sub>@PSPMK-DS. Subsequently, the rats started a running exercise on a level treadmill at a speed of 60 km h<sup>-1</sup> for 1 h every other day in order to induce osteoarthritis at the knee joint.

**X-Ray Radiograph and Histological Staining Analyses:** At one and eight weeks after surgery, the rats were scanned using an X-ray imager for small animals (Faxitron X-ray, USA) with the voltage of 32 kV and the exposure time of 6 mAs. After scanning, the rats were sacrificed and their knee joints were fixed in 4% paraformaldehyde for 24 h and decalcified in 10% EDTA. The macroscopic cartilage lesion depth for each group was measured by a Vernier caliper. Afterward, the samples were dehydrated and embedded within paraffin, and then serial paraffin sections with a thickness of 5  $\mu$ m were prepared and stained alternately with H&E and safranin O-fast green. The safranin O-fast green sections were evaluated utilizing the Osteoarthritis Research Society International (OARSI) score established by Pritzker et al.,<sup>39</sup> which scored the product of six grades (depth of lesion) and four stages (extent of involvement) on a scale of 0 (normal) to 24 (severe osteoarthritis). Digital images were captured and two authors (Yan and Qi) graded the sections independently. The relative glycosaminoglycan content was also measured based on the safranin O staining using Image J software.

Statistical Analysis: The data were shown as mean  $\pm$  standard deviation (SD), and similar independent experiments were repeated at least three times with three replicates to verify the results. One-way analysis of variance (ANOVA) was used for the multiple comparison tests. A two-tailed nonpaired Student's t-test was employed to compare the significant differences between two groups, and statistical significance was displayed as \*P < 0.05, \*\* P < 0.01, or \*\*\* P < 0.001; #P < 0.05, ##P < 0.01, or ###P < 0.001.

## Acknowledgements

Y.Y., T.S., and H.Z. contributed equally to this work. This study was financially supported by National Key Research and Development Program of China (2018YFC1106200 and 2018YFC1106204), National Natural Science Foundation of China (51675296, 51873107, and 81572099), Ng Teng Fong Charitable Foundation (202-276-132-13), Research Fund of State Key Laboratory of Tribology, Tsinghua University, China (SKLT2018B08), Shanghai Science and Technology Commission (18ZR1434200 and 17140900102), Shanghai Municipal Education Commission—Gaofeng Clinical Medicine Grant Support (20171906), Shanghai Jiao Tong University “Medical and Research” Program (ZH2018ZDA04), and Major Program for the Fundamental Research of Shanghai (2014ZYJB0302). H.Z. acknowledges financial support from Jane and Aatos Erkkö Foundation (grant no. 4704010), Academy of Finland (grant no. 297580), and Sigrid Jusélius Foundation (decision no. 28001830K1). Prof. H. A. Santos acknowledges financial support from the HiLIFE Research Funds and the Sigrid Jusélius Foundation (decision no. 4704580).

## Conflict of Interest

The authors declare no conflict of interest.

## Reference

- [1] G. Liu, M. Cai, F. Zhou, W. Liu, *J. Phys. Chem. B* 2014, 118, 4920.
- [2] T. Sun, Y. L. Sun, H. Y. Zhang, *Polymers* 2018, 10, 513.
- [3] S. N. Jha, R. P. Kachru, *J. Food Process Eng.* 1998, 21, 301.
- [4] M. Shankar, N. Chaudhary, D. Singh, *Int. J. Pharm. Biol. Arch.* 2010, 1, 101.
- [5] Q. Zhang, F. Liu, K. T. Nguyen, X. Ma, X. Wang, B. Xing, Y. Zhao, *Adv. Funct. Mater.* 2012, 22, 5144.
- [6] L. He, Y. Huang, H. Zhu, G. Pang, W. Zheng, Y. S. Wong, T. Chen, *Adv. Funct. Mater.* 2014, 24, 2754.
- [7] C. de la Torre, I. Casanova, G. Acosta, C. Coll, M. J. Moreno, F. Albericio, E. Aznar, R. Mangues, M. Royo, F. Sancenón, R. Martínez-Mañez, *Adv. Funct. Mater.* 2015, 25, 687.
- [8] L. Palanikumar, E. S. Choi, J. Y. Cheon, S. H. Joo, J. H. Ryu, *Adv. Funct. Mater.* 2015, 25, 957.
- [9] W. Ngamcherdtrakul, J. Morry, S. Gu, D. J. Castro, S. M. Goodyear, T. Sangvanich, M. M. Reda, R. Lee, S. A. Mihelic, B. L. Beckman, Z. Hu, J. W. Gray, W. Yantasee, *Adv. Funct. Mater.* 2015, 25, 2646.

- [10] Z. Li, J. Barnes, A. Bosoy, J. F. Stoddart, J. Zink, *Chem. Soc. Rev.* 2012, 41, 2590.
- [11] Y. L. Sun, H. Y. Zhang, Y. X. Wang, Y. Wang, *J. Controlled Release* 2017, 259, e45.
- [12] Y. Sun, Y. Yang, *J. Controlled Release* 2013, 8, 181.
- [13] Z. Qu, H. Xu, H. Gu, *ACS Appl. Mater. Interfaces* 2015, 7, 14537.
- [14] T. Ribeiro, E. Coutinho, A. S. Rodrigues, C. Baleizão, J. P. S. Farinha, *Nanoscale* 2017, 9, 13485. [15] D. R. Radu, C. Y. Lai, J. W. Wiench, M. Pruski, V. S. Lin, *J. Am. Chem. Soc.* 2004, 126, 1640.
- [16] C. Boyer, N. A. Corrigan, K. Jung, D. Nguyen, T. K. Nguyen, N. M. Adnan, S. Oliver, S. Shanmugam, J. Yeow, *Chem. Rev.* 2016, 116, 1803.
- [17] J. Klein, *Science* 2009, 323, 47.
- [18] S. Jahn, J. Seror, J. Klein, *Annu. Rev. Biomed. Eng.* 2016, 18, 235.
- [19] J. Klein, *Friction* 2013, 1, 1.
- [20] J. Seror, L. Zhu, R. Goldberg, A. J. Day, J. Klein, *Nat. Commun.* 2015, 6, 6497.
- [21] M. Kobayashi, A. Takahara, *Chem. Rec.* 2010, 10, 208.
- [22] J. Seror, Y. Merkher, N. Kampf, L. Collinson, A. J. Day, A. Maroudas, J. Klein, *Biomacromolecules* 2011, 12, 3432.
- [23] G. Liu, Z. Liu, N. Li, X. Wang, F. Zhou, W. Liu, *ACS Appl. Mater. Interfaces* 2014, 6, 20452.
- [24] M. Kobayashi, M. Terada, A. Takahara, *Faraday Discuss.* 2012, 156, 403.
- [25] X. Zhu, C. Yan, F. M. Winnik, D. Leckband, *Langmuir* 2007, 23, 162.
- [26] J. Israelachvili, *Intermolecular and surface forces*, 2nd ed., Academic Press, San Diego, CA 1991.
- [27] H. Iijima, T. Aoyama, A. Ito, J. Tajino, M. Nagai, X. Zhang, S. Yamaguchi, H. Akiyama, H. Kuroki, *Osteoarthritis Cartilage* 2014, 22, 1036.
- [28] Y. Sun, B. Yang, S. X. Zhang, Y. Yang, *Chem. - Eur. J.* 2012, 18, 9212.
- [29] Y. Sun, Y. Yang, D. Chen, G. Wang, Y. Zhou, C. Wang, J. F. Stoddart, *Small* 2013, 9, 3224.
- [30] H. Y. Zhang, Y. F. Sun, Y. L. Sun, M. Zhou, *Bio-Med. Mater. Eng.* 2014, 24, 2211.
- [31] Y. Wang, W. G. Cui, X. Zhao, S. Z. Wen, Y. L. Sun, J. M. Han, H. Y. Zhang, *Nanoscale* 2018, <https://doi.org/10.1039/C8NR07329E>.
- [32] F. Sun, Y. Li, N. Zhang, J. Nie, *Polymer* 2014, 55, 3656.
- [33] H. Y. Zhang, J. B. Luo, M. Zhou, Y. Zhang, Y. L. Huang, *J. Mech. Behav. Biomed. Mater.* 2013, 20, 209.
- [34] H. Y. Zhang, S. H. Zhang, J. B. Luo, Y. H. Liu, S. H. Qian, F. H. Liang, Y. L. Huang, *J. Tribol.* 2013, 135, 032301.
- [35] H. Y. Zhang, Y. J. Zhu, X. Y. Hu, Y. F. Sun, Y. L. Sun, J. M. Han, Y. Yan, M. Zhou, *Bio-Med. Mater. Eng.* 2014, 24, 2151.
- [36] Y. Y. Jiao, S. Z. Liu, Y. L. Sun, W. Yue, H. Y. Zhang, *Langmuir* 2018, 34, 12436.
- [37] A. Mirando, Y. Dong, J. Kim, *Methods Mol. Biol.* 2014, 1130, 267.
- [38] C. Li, K. Chen, H. Kang, *Cell Death Dis.* 2017, 8, e3165.
- [39] K. P. H. Pritzker, S. Gay, S. A. Jimenez, K. Ostergaard, J. P. Pelletier, P. A. Revell, D. Salter, W. B. van den Berg, *Osteoarthritis Cartilage* 2006, 14, 13